



# Mode III threshold under Rolling Contact Fatigue and development of a test gearbox for planet gears

## Conference Proceedings

Prasad Mahendra Rao<sup>1</sup> · Stefano Foletti<sup>1</sup> · Luca Bonaiti<sup>1</sup> · Franco Concli<sup>2</sup> · Carlo Gorla<sup>1</sup> · Stefano Beretta<sup>1</sup>

Received: 13 April 2021 / Accepted: 11 October 2021 / Published online: 14 January 2022

© The Author(s), under exclusive licence to Springer-Verlag GmbH Deutschland, ein Teil von Springer Nature 2021

### Abstract

This paper is on the assessment for Mode III crack propagation under the influence of primarily Rolling Contact Fatigue (RCF) in integrated thin-rimmed planetary gears and its integrated bearings, and the design and development of a test gearbox for the full-scale testing of such a 3-gear train planet gears layout. It is in response to the ‘Innovative DEsign for Reliable PLANet bearings’ (IDERPLANE) research project which will address the concern of high RCF in planetary gear bearings in the epicyclic modules of aerospace applications such as Geared turbofans (GTFs) and Main gearboxes (MGBs) in aircrafts. The project is part of the Clean Sky 2 Horizon 2020 call, and its consortium is headed by the Politecnico di Milano.

## Mode III Rißausbreitung: Entwicklung eines Testgetriebes für Planetenräder

Tagungsband

### Zusammenfassung

Dieser Beitrag konzentriert sich auf die Bewertung der Mode-III-Rißausbreitung unter dem Einfluss von Kontaktermüdung (RCF) in integrierten dünnrandigen Planetenradlagern und die Konstruktion und Entwicklung eines Testgetriebes. Die Ergebnisse wurden im Rahmen des Forschungsprojekts „Innovative DEsign for Reliable PLANet bearings“ (IDERPLANE) gewonnen. Das Projekt konzentriert sich auf das Versagen von integrierten Planetenradlagern in den Umlaufmodulen von Luft- und Raumfahrtanwendungen wie Getriebefans (GTFs) und Hauptgetrieben (MGB) von Flugzeugen. Das Projekt ist Teil des Clean Sky 2 Horizon 2020 Calls, dessen Konsortium vom Politecnico di Milano geleitet wird.

## 1 Mixed mode crack propagation

Mixed mode crack propagation in planet gears with integrated bearings, particularly in the roller-race interface region, is a complex scenario; to fully address it, a mixed approach based on both, numerical simulations and ex-

perimental tests is needed. The main goal of this present research project is to apply existing literature approaches [1–6] to a planetary-type gear to study the behaviour of subsurface cracks at the roller-race interface that can lead to either spalling, or also in-core propagation, leading to gross failure. All such subsurface cracks start nucleation in Mode III, and after considerable propagation, can branch off into Mode I. Hence the focus is on Mode III threshold properties.

---

✉ Prasad Mahendra Rao  
prasadmahendra.rao@polimi.it

<sup>1</sup> Department of Mechanical Engineering, Politecnico di Milano, Milan, Italy

<sup>2</sup> Faculty of Science and Technology, Libera Università di Bolzano, Bolzano, Italy

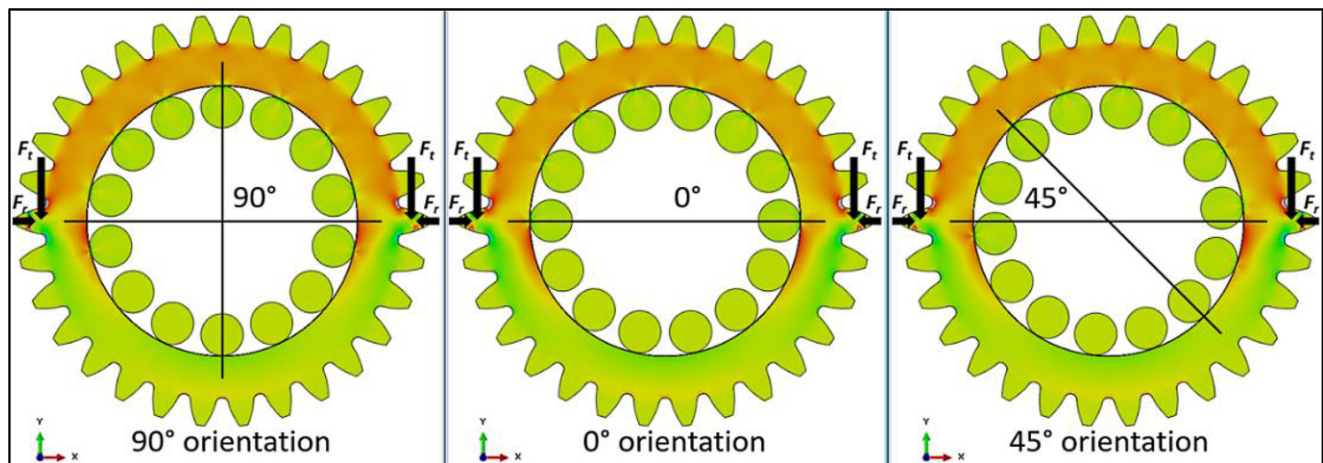


Fig. 1 FE analysis depicting the hoop stress for all proposed orientations of the rollers

## 2 Assessing the stress state for Mode III crack propagation

Initially, a preliminary analysis that aims to define the complex stress state at, and below the surface at the roller-race interface along the inner rim of the thin rimmed main planet gear is discussed. To account for the actual service conditions at said interface, influences from multiple stress contributions such as: Hertzian contact stresses, edge loading effect, ovalization of gear, and fatigue cycles including the effective stress ratio have been considered, being exhaustive. The baseline gear material is an aerospace-grade high speed bearing steel, while the bearing components in the planetary gear bearing (test article) come from a standard cylindrical roller bearing from Schaeffler.

The above-mentioned loading conditions are applied to the planet gear under assessment in a Finite Element (FE) environment. Since RCF is a multiaxial out-of-phase (MOOP) loading condition, the relations of proportions and phases are the most important. These relations will then be used as input for the experimental campaign to determine the Mode III stress intensity factor (SIF) threshold under RCF. In our case, the bearing profile is logarithmic, so the most critical zone is the one at the center, and a preliminary 2D FE analysis captures this zone of interest well. Subsequently, a 3D FE analysis will be performed to correlate the results with the full-scale test articles of the experimental campaign. Friction has been neglected in the analysis since we are in full-lubricated conditions and the gears are of the spur type. The analysis has been performed in a 2D plain strain non-linear condition (CPE8), with local and global seed element sizes that have been verified to give convergence for the analysis. A finer mesh has been used at and below the surface to a depth up to which all the stress components have a significant influence. Both, the tangential and radial gear pair loads (Fig. 1) have been

applied, and the target contact pressure at the roller-race interface is achieved.

Three different orientations for the position of the roller-cage assembly have been assessed to determine the most detrimental one: these are the position of any one of the rollers at  $90^\circ$ ,  $0^\circ$  or  $45^\circ$  (Fig. 1). While, during in-service conditions, the cage along with its rollers could be in any of the spatial positions, but the most damaging condition is one of these three only.

In Fig. 1, we see the distribution of the hoop stresses along the test article for all the three orientations (the depicted distribution is within the same limits for all graphs). This peculiar pattern, inherent in such thin-rimmed gears, is attributed to the phenomenon of ovalization which is due to the considerable bending moments generated due to the gear loads in the thin-rimmed section of the planet gear. It has a substantial damaging effect in addition to the existing scenario with the Hertzian contact stresses.

In presence of defects, the assessment can be performed based either on Linear Elastic Fracture Mechanics principles or fatigue failure criteria in presence of defects. There exist two types of treatments for RCF in literature: the first calculates the SIF at defect tips and compares it with the stress intensity factor range,  $\Delta K_{Ih}$ , under Mode II/III. The other employs the use of a fatigue criterion where the fatigue limit depends on the defect size, assuming, as per Murakami's [10] concept that defects can be treated as small cracks. The details of these methods, and the basis for the present approach is detailed in [4].

Now, the Dang Van multiaxial high-cycle fatigue criterion [7–9] is extensively applied in the assessment of MOOP loading conditions, hence also RCF. It outputs an equivalent allowable shear stress ( $\tau_{DV}$ ) as a function of the hydrostatic stress ( $\sigma_h$ ). It is an application based on elastic shakedown principles at the mesoscopic scale.

**Fig. 2** Stress state for 90° orientation plotted on the modified Dang Van plane

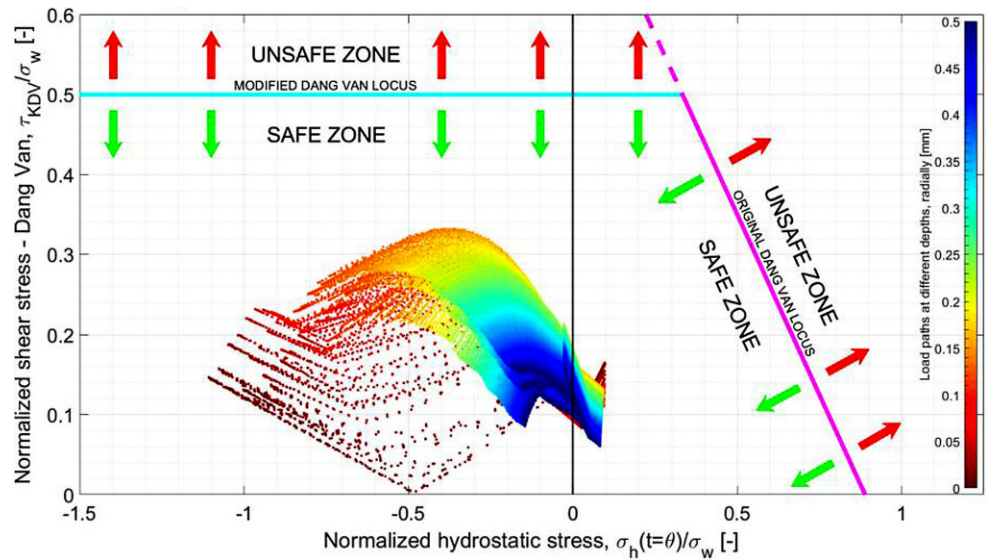
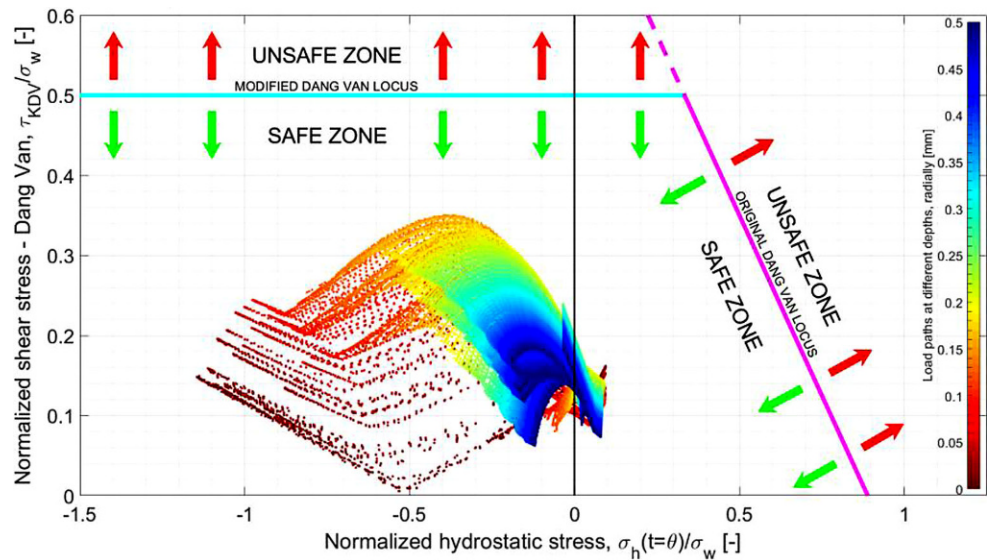


**Fig. 3** Stress state for 0° orientation plotted on the modified Dang Van plane



The Dang Van criterion can be expressed as:

$$\tau_{DV}(t) + \alpha_{DV} \cdot \sigma_h(t) \leq \tau_w \tag{1}$$

where:  $\tau_w$  is the fatigue limit in reversed torsion;  $\sigma_h(t)$  is the instantaneous hydrostatic component of the stress tensor; and  $\tau_{DV}(t)$  is the instantaneous value of the Tresca shear stress, given by:

$$\tau_{DV}(t) = \frac{\widehat{s}_I(t) - \widehat{s}_{III}(t)}{2} \tag{2}$$

evaluated over a symmetrized stress deviator found at the mesoscopic scale, obtained by subtracting from the deviatoric stress,  $s_{ij}(t)$ , a constant tensor,  $s_{ij,m}$ , given by:

$$\widehat{s}_{ij}(t) = s_{ij}(t) - s_{ij,m} \tag{3}$$

where:  $s_{ij,m}$  is a residual stress deviator, that fulfills the condition of an elastic shakedown state at the mesoscopic scale.  $\alpha_{DV}$  is a material parameter, calibrated with two fatigue tests; tension-compression to obtain  $\sigma_w$ , and torsion to obtain  $\tau_w$ :

$$\alpha_{DV} = 3 \cdot \left( \frac{\tau_w}{\sigma_w} - \frac{1}{2} \right) \tag{4}$$

The relationship between the fatigue limit and the defect size (Kitagawa diagram) has been obtained through a series of axial or bending fatigues tests at a stress ratio,  $R = -1$  on micro-notched and smooth specimens. These experimental

**Fig. 4** Stress state for 45° orientation plotted on the modified Dang Van plane

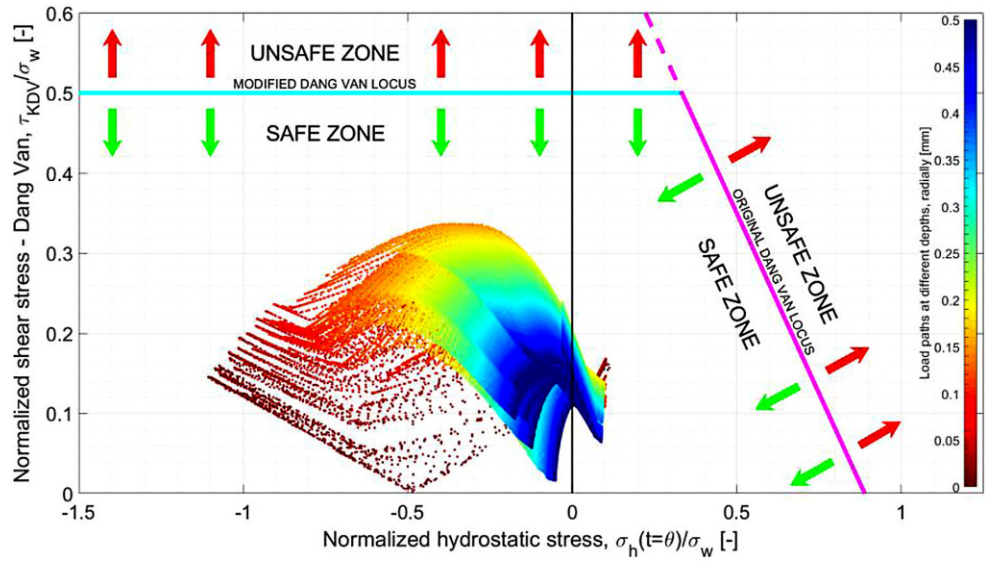
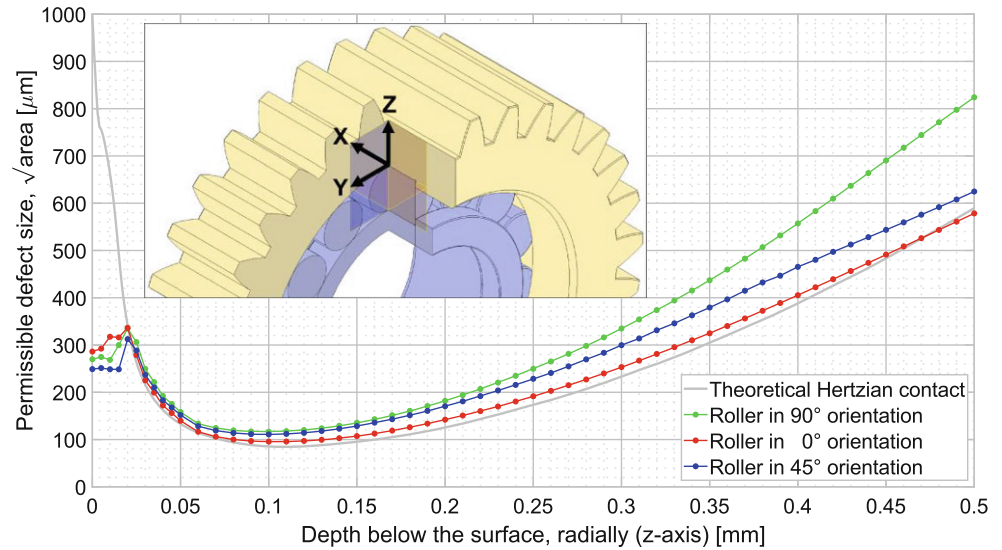


**Fig. 5** Defect acceptance map implementing the modified Dang Van criterion



results were interpolated by means of the modified El-Haddad [12] model:

$$\sigma_w = \sigma_{w0} \cdot \sqrt{\frac{\sqrt{area_0}}{\sqrt{area} + \sqrt{area_0}}} \tag{5}$$

where:  $\sigma_{w0}$  is the fatigue limit for smooth specimens,  $\sigma_w$  is the fatigue limit depending on the defect size (expressed in terms of Murakami’s  $\sqrt{area}$  parameter) and  $\sqrt{area_0}$  is the fictitious crack length for different defect sizes obtained by interpolating on the fatigue limit.

The results from the FE analysis are used to plot the stress state on the Dang Van ( $\tau_{DV}-\sigma_h$ ) plane for all the orientations of 90°, 0° and 45° in Figs. 2, 3 and 4 respectively. The published data has been normalized with respect to the axial fatigue limit,  $\sigma_w$ . The resulting failure locus is represented by a line (Original Dang Van Locus) [7–9].

Now, to avoid a non-conservative prediction in RCF, the modified Dang Van criterion [11], is implemented that proposes that in the region with  $\sigma_h < 0$ , the failure locus (Modified Dang Van Locus) is a constant value,  $\tau_w = 0.5\sigma_w$ :

$$\tau_{DV}(t) \leq \tau_w = \frac{\sigma_w}{2} \text{ if } \sigma_h < 0 \tag{6}$$

The stress state plotted in this plane is plotted at different depths, starting from the surface, and then moving radially deeper into the material away from the roller-race interface all along the periphery. A denser population of points is present near the surface to capture the behaviour in detail near the surface. Hence the plot considers the stress state at all locations, that is, at each given roller position, at a given radial coordinate.

Lastly, a *defect acceptance map* that plots the permissible defect size as a function of the depth below the surface that



does not lead to Mode II/III crack propagation using this modified Dang Van criterion is plotted in Fig. 5.

From Figs. 2, 3, 4 and 5 of the Dang Van planes and the defect acceptance map, it is observed that amongst the three orientations, the one at  $0^\circ$  is the most severe as it leads to the lowest permissible defect size below the surface. While differently, the orientation of  $45^\circ$  is more damaging for the initial  $20\mu\text{m}$  (this can be attributed to the asymmetry of the positioned rollers in this orientation). The depth of  $0.1\text{--}0.15\text{mm}$  below the surface is the most critical depth which is in line with Hertzian contact theory for metals. The capture of this peculiar behaviour in the initial depth of the material was possible due to a fine mesh in that region; and this becomes evident from the defect acceptance map.

Also, the extent of damage that is inflicted when the specimen is a thin-rimmed planet gear as compared to a similar theoretical Hertzian contact is also envisaged through Fig. 5. Here, for the theoretical Hertzian contact at the interface region of the most loaded roller and the race under same loading conditions, the permissible defect size near the surface is considerably higher when compared with our specimen under similar conditions, while at the critical depth approaches the same value for both cases. This initially lower value signifies a more damaging mechanism due to the phenomenon of ovalization in thin-rimmed gears, and this exercise has helped us quantify its effect and extent in our case.

Hence, the above numerical results are used as input for running the multiaxial fatigue tests on standard specimens in a loading condition equivalent to this real one. The multiaxial tests are performed on an MTS 809 Axial/Torsional Test System ( $250\text{kN}/2200\text{Nm}$ ). The experimental results are then used to determine the Mode III SIF threshold un-

der RCF for this material. From our experimental campaign, we have achieved the ratio for  $\Delta K_{III}/\Delta K_{th,I}$  to be less than 1. Hence, in this giving loading condition, which can be considered a loading condition equivalent to RCF, the crack indeed starts nucleation and propagation in Mode III. It was observed that after substantial crack propagation under Mode III, the leading edge of the crack tip did show a tendency to branch off under Mode I.

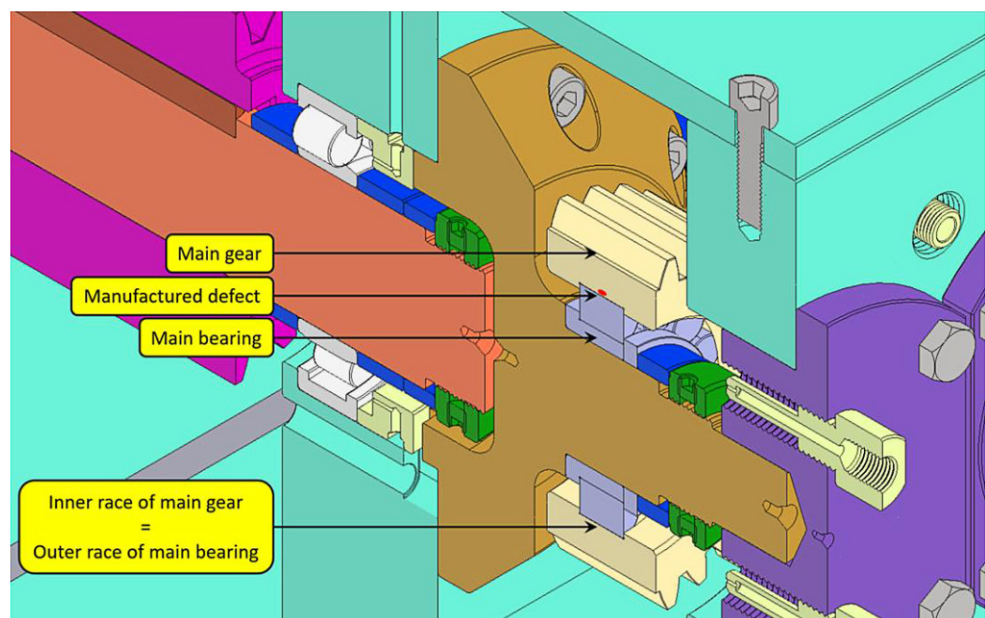
### 3 Applying findings to full-scale tests for validation

The proposed approach, based on simplified experimental tests on standard specimens where the real loading condition cannot be fully addressed, will be validated, for the first time in literature with full-scale experimental campaigns under service load conditions on test articles.

Hence, a new test gearbox on a modified test rig has been designed and developed to study this phenomenon. The torque required for simulating such full-scale fatigue tests is provided by a power recirculating-type [Forschungsstelle für Zahnräder und Getriebebau (FZG)-type] gear test rig in our facility, used conventionally for the testing of two gears. Here the core RCF test will itself get performed due to the design of the intended test gearbox coupled to the test rig system.

Post completion of the test gearbox development, and when its interfacing with the test rig system is complete, the final criteria is to have a defect introduced at the contact interface of the inner race (rim) of the planet gear and the rollers of its integrated bearing to simulate subsurface defects as discussed earlier (Fig. 6).

**Fig. 6** Intended final criteria for the test gearbox



## 4 Gearbox design philosophy

For the design and development of the said test gearbox, the conventional 2-gear train layout is replaced by an equivalent 3-gear train layout that intends to simulate similar drive conditions as those that would specifically be encountered by a full-scale planetary gear bearing present in the epicyclic module of high-power mechanical power transmission systems of aerospace applications. The design solution is envisaged in such a way so that the integration of the test gearbox with the rest of the test rig remains unchanged. In Fig. 7, the slave gearbox (left) remains the same while the test gearbox (right) will be replaced by the new test gearbox. Constraints on the design were imposed by the following challenges: the existing test rig mounting

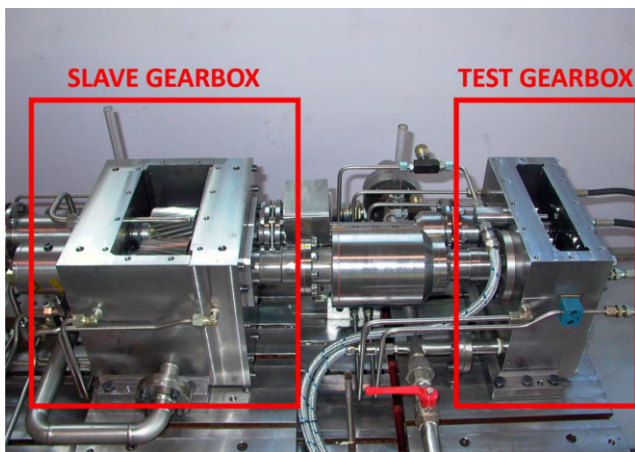
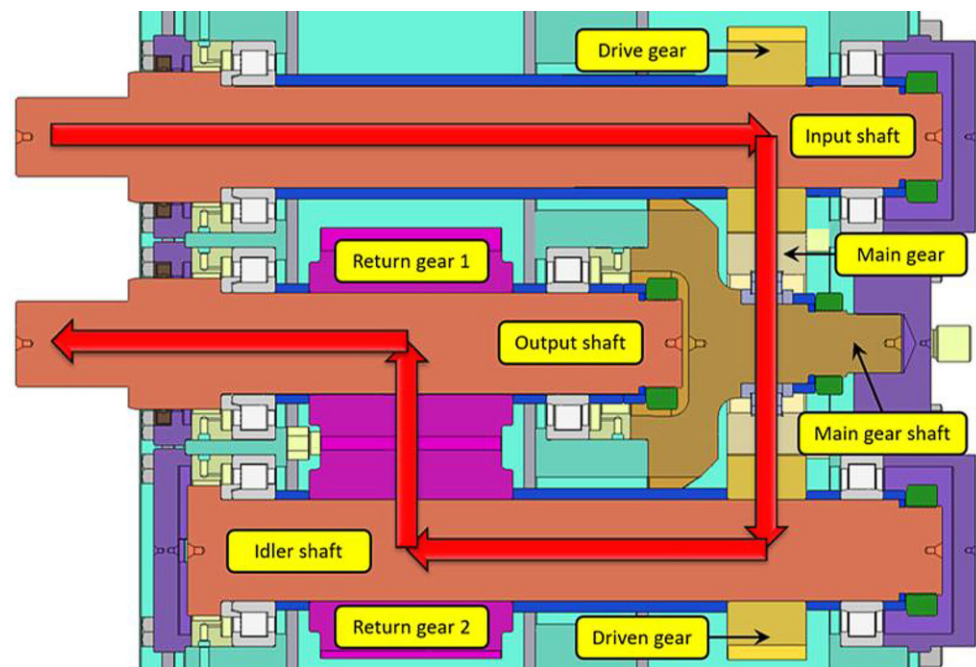


Fig. 7 Layout of the entire test rig

Fig. 8 Spatial layout and flow of drive through the system



points, the strength of gears in the system, and the standard bearing that is part of the test article. Since the new test gearbox will be coupled to the slave gearbox of the test rig, the input-output shaft center distances have been emulated for simplicity. All gears in the 3-gear train (that includes the test article operating as an idler gear in the middle) have been kept geometrically identical for a uniform stress distribution, this also aided in a more compact packaging solution (Fig. 8). Lubrication is of the splash and oil jet-type with dedicated supply to all critical components such as the bearings and the locations at which the gears mesh.

All the gears in the system have been designed as standard module and pressure spur gears following ISO 6336 and have been optimized using a parametric tool to ensure highest possible transmission capabilities and safety factors. For all gears, the design was aimed to maximize the root safety ( $S_F$ ) and flank safety ( $S_H$ ) factors. While to size the test gearbox, the target was to ensure that the stress state subjected to the test article bearing is similar to full-scale benchmark conditions.

As mentioned before, the bearing that would be integrated into the test article gear is a standard cylindrical bearing from Schaeffler; its geometry also posed a constraint to the design of the test gearbox. On assembly, this bearing would lose its standard outer race and would be replaced by the planet gear itself which would have the mating race machined onto its inner rim (Fig. 6).

All the components have been assessed to ensure longevity of the whole test gearbox system. Special attention has been taken by means of adequate gear modifications to ensure that the quality and efficiency of the gear

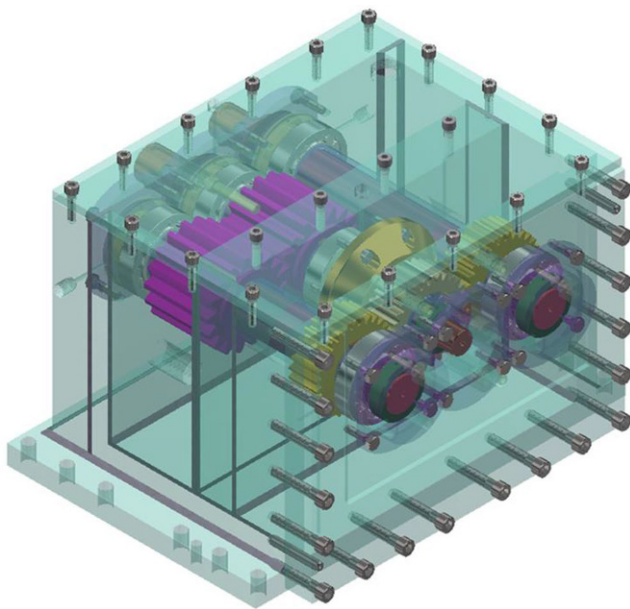
**Table 1** Test rig and test gearbox specifications

Parameter [units]	Value
Maximum torque (system) [Nm]	800
Maximum speed [RPM]	3000
Lubrication type; oil-type [-]	Oil injection; mineral-oil base
Service oil temperature [°C]	70
Overall gear ratio for test gearbox [-]	17/18
<b>Full-scale test article details</b>	
Gear ratio for 3-gear train [-]	1:1
Center distance (= pitch circle diameter) [mm]	91.5
Normal module [mm] and pressure angle [°]	3 (spur) and 20
Face width [mm]	35
Gear reference profile [-]	1.25/0.38/1.0 ISO 53:1998 Profil A

drive and their life is not adversely affected by the shaft deflections due to the positions of the gears on the shafts itself.

The housing structure is a weldment assembly, precision machined on assembly, and the whole design project has followed Design for X principles to ensure a quality and reliable product. The schematic layout of the test gearbox is shown in Fig. 9, and is currently under manufacturing.

Post the full-scale test campaign on the test rig, its experimental results will be used to validate the use of the modified Dang Van multiaxial fatigue criterion, specifically suited for this multiaxial stress state comprising of RCF and aforementioned stress components, for obtaining an initial estimation of the permissible critical defect size at the roller-race interface for applications in the heavy engineering sector.

**Fig. 9** Complete view of the gearbox

**Acknowledgements** This project has received funding from the Clean Sky 2 Joint Undertaking under the European Union's Horizon 2020 research and innovation programme under grant agreement no. 821315.

## References

### Cited Literature

- Beretta S, Foletti S, Valiullin K (2011) Fatigue strength for small shallow defects/cracks in torsion. *Int J Fatigue* 33(3):287–299
- Tarantino MG, Beretta S, Foletti S, Lai J (2011) A comparison of Mode III threshold under simple shear and RCF conditions. *Eng Fract Mech* 78(8):1742–1755
- Tarantino MG, Beretta S, Foletti S, Papadopoulos I (2013) Experiments under pure shear and rolling contact fatigue conditions: Competition between tensile and shear mode crack growth. *Int J Fatigue* 46:67–80
- Foletti S, Beretta S, Tarantino MG (2014) Multiaxial fatigue criteria versus experiments for small crack under rolling contact fatigue. *Int J Fatigue* 58:181–192
- Foletti S, Beretta S, Gurer G (2016) Defect acceptability under full-scale fretting fatigue tests for railway axles. *Int J Fatigue* 86:34–43
- Conrado E, Foletti S, Gorla C, Papadopoulos IV (2011) Use of multi-axial fatigue criteria and shakedown theorems in thermo-elastic rolling-sliding contact problems. *Wear* 270(5–6):344–354
- Van Dang K, Cailletaud G, Flavenot JF, Le Douaron A, Lieurade HP (1989) Criterion for high cycle fatigue failure under multi-axial loading. In: Brown MW, Miller KJ (eds) *International Conference on Biaxial/Multi-axial Fatigue*. Biaxial and multi-axial fatigue EGF, vol 3. Mechanical Engineering Publications, London, pp 459–478
- Van Dang K, Griveau B, Message O (1989) On a new multi-axial fatigue limit criterion: theory and application. In: Brown MW, Miller KJ (eds) *International Conference on Biaxial/Multi-axial Fatigue*. Biaxial and multi-axial fatigue EGF, vol 3. Mechanical Engineering Publications, London, pp 479–496
- Van Dang K (1993) Macro-micro approach in high-cycle multi-axial fatigue. In: McDowell DL, Ellis R (eds) *Advances in Multi-axial Fatigue*, ASTM STP 1191, Philadelphia, pp 120–130
- Murakami Y (2002) *Metal fatigue: effects of small defects and non-metallic inclusions*. Elsevier, Oxford
- Desimone H, Bernasconi A, Beretta S (2006) On the application of Dang Van criterion to rolling contact fatigue. *Wear* 260.4:567–572
- El Haddad MH, Smith KN, Topper TH (1979) Fatigue crack propagation of short cracks. *J Eng Mater Technol* 101(1):42–46

### Further Reading

- Depouhon P, Sola C, Descharrières B, Delabie A (2017) A stress based critical-plane approach for study of rolling contact fatigue crack propagation in planet gears. Airbus. <http://hdl.handle.net/20.500.11881/3831>
- Niemann G, Winter H, Höhn B-R (2006) *Manuale degli organidelle macchine* (Tecnica Nuove)
- Harris TA (2001) *Rolling bearing analysis*. John Wiley & Sons Inc., Hoboken
- Langstreth Johnson K (1985) *Contact mechanics*. University Press, Cambridge
- ISO 6336-series:2019. Calculation of load capacity of spur and helical gears—Multiple parts. Standard. Geneva, CH: International Organization for Standardization, Nov. 2019.
- ISO/TS 16281:2008. Rolling bearings—Methods for calculating the modified reference rating life for universally loaded bearings.

- Standard. Geneva, CH: International Organization for Standardization, June 2008.
19. ISO281:2007. Rolling bearings—Dynamic load ratings and rating life. Standard. Geneva, CH: International Organization for Standardization, Feb. 2007.